Morphotropic Phase Boundary in the Pb-Free $(1-x)BiTi_{3/8}Fe_{2/8}Mg_{3/8}O_3$–$xCaTiO_3$ System: Tetragonal Polarization and Enhanced Electromechanical Properties

Pranab Mandal, Alicia Manjón-Sanz, Alex J. Corkett, Tim P. Comyn, Karl Dawson, Timothy Stevenson, James Bennett, Leonard F. Henrichs, Andrew J. Bell, Eiji Nishibori, Masaki Takata, Marco Zanella, Michelle R. Dolgos, Umut Adem, Xinming Wan, Michael J. Pitcher, Simon Romani, T. Thao Tran, P. Shiv Halasyamani, John B. Claridge, and Matthew J. Rosseinsky**

The perovskite oxide lead zirconate titanate ($PbZr_{1-x}Ti_xO_3$) (PZT) has extraordinary electromechanical properties at the morphotropic phase boundary (MPB),[1] making modified PZT ceramics the basis for almost all actuators, sensors and related applications in use today. The MPB in the PZT solid solution occurs near $x \approx 0.48$[1] between the ferroelectric rhombohedral (*R*3*m*, denoted as $R_{[111]}$) and tetragonal (*P*4*mm*, denoted as $T_{[001]}$) phases, with polarizations lying along the $[111]_p$ body diagonal and $[001]_p$ edge of the primitive ≈ 4 Å ABO_3 perovskite unit cell, respectively.[1–3] The PZT phases are untilted and the $R_{[111]}$ and $T_{[001]}$ structures are described crystallographically, using a modified Glazer notation, as $a^0_+a^0_+a^0_+$ and $a^0_0a^0_0c^0_+$, respectively, where the subscript indicates ferroelectric displacement and the superscript the nature of the octahedral tilting with respect to the primitive unit cell axes.[4] It is challenging to create an MPB in a bismuth-based lead-free system as it has proved difficult to prepare phases with polarization directed along the $[001]_p$ primitive cell edge in such materials. Several Pb-free MPB systems based on $K_{0.5}Na_{0.5}NbO_3$, $Na_{0.5}Bi_{0.5}TiO_3$ (NBT), $BaTiO_3$ (BTO), and $K_{0.5}Bi_{0.5}TiO_3$ (KBT) are known but all have inferior properties to PZT.[2,3,5] Bi^{3+} has a $6s^2$ configuration with crystal chemistry similar to that of Pb^{2+}, and bismuth-based perovskites are attractive as they can offer high Curie and depolarization temperatures required for demanding application environments.[5,6] A phase with $[001]_p$ polarization that is accessible at ambient pressure with a high (>50%) Bi^{3+} content is thus a significant target.

There are very few bismuth perovskites such as $BiFeO_3$ (*R*3*c*) which can be stabilized at ambient pressure. We have developed a strategy based on multiple B site cations to access such materials, e.g., antiferroelectric $Bi_2Mn_{4/3}Ni_{2/3}O_6$[7] and the polar rhombohedral ($R_{[111]}$) phase $BiTi_{3/8}Fe_{2/8}Mg_{3/8}O_3$ (BTFM), which has a high Curie temperature of 730 °C.[8] In BTFM, in addition to the long-range ordered $[111]_p$ displacements, the Bi cations have locally correlated $[110]_p$ displacements[9] which can be converted into a long-range polarization along this direction by the introduction of $LaFeO_3$ (LFO) which itself has antiferrodistortive $[110]_p$ displacements, although this orthorhombic $O_{[110]}$

Dr. P. Mandal, Dr. A. Manjón-Sanz, Dr. A. J. Corkett, Dr. M. Zanella, Dr. M. R. Dolgos, Dr. U. Adem, Dr. X. Wan, Dr. M. J. Pitcher, Dr. J. B. Claridge, Prof. M. J. Rosseinsky
Department of Chemistry
University of Liverpool
Liverpool L69 7ZD, UK
E-mail: j.b.claridge@liv.ac.uk; m.j.rosseinsky@liv.ac.uk

Dr. A. Manjón-Sanz, Prof. E. Nishibori, Prof. M. Takata
Structural Materials Science Laboratory
RIKEN SPring-8 Center, 1-1-1, Kouto, Sayo-cho, Sayo-gun, Hyogo 679-5148, Japan

Dr. T. P. Comyn, Dr. T. Stevenson, Dr. J. Bennett, L. F. Henrichs, Prof. A. J. Bell
Institute for Materials Research
University of Leeds
Leeds, LS2 9JT, UK

Dr. K. Dawson, Dr. S. Romani
Centre for Materials and Structures
School of Engineering
University of Liverpool
Liverpool, L69 3GH, UK

Prof. E. Nishibori
Division of Physics
Faculty of Pure and Applied Sciences
CiRfSE and TIMS
University of Tsukuba
1-1-1 Tennodai, Tsukuba, Ibaraki 305-8571, Japan

Prof. M. Takata
Japan Synchrotron Radiation Research Institute (JASRI)
1-1-1, Kouto, Sayo-cho, Sayo-gun, Hyogo 679-5198, Japan

Prof. M. Takata
Department of Advanced Materials Science
The University of Tokyo
5-1-5 Kashiwanoha, Kashiwa-shi, Chiba 277-8561, Japan

T. T. Tran, Prof. P. S. Halasyamani
Department of Chemistry
University of Houston
Houston, TX 77204-5003, USA

DOI: 10.1002/adma.201405452

phase is separated from $R_{[111]}$ BTFM by a non-perovskite region of the phase diagram.[10] We therefore explored solid solutions between BTFM and $CaTiO_3$ (CTO), motivated by the isostructural nature of LFO and CTO, but noting that the Ti cation in BTFM undergoes local displacements along multiple directions[9] that are not correlated with the primary $[111]_p$ A-site displacement direction favored by the other two B site cations. This enhances the likelihood of locking in other long-range polarization directions when Ti rather than Fe is the B site cation introduced by solid solution formation and may enable the two perovskite symmetries to directly neighbor each other in the phase diagram. We obtain a Bi-based perovskite $O_{[001]}$ phase with polarization along $[001]_p$ and accessible at ambient pressure. Enhanced piezoelectric properties and high depolarization temperatures are observed in the wide MPB region formed with an R phase, with up to 92.5% Bi on the perovskite A site.

Solid solutions $(1 - x)$BTFM–xCTO were synthesized successfully in the range $0.0 < x \leq 0.40$ (the perovskite structure is maintained over this entire composition range in contrast with BTFM–LFO[10]). The $R_{[111]}$ powder X-ray diffraction (PXRD) pattern of BTFM changes dramatically with increasing CTO content beyond $x = 0.05$, as shown in **Figure 1** (also Figure S1, Supporting Information). A complex PXRD pattern emerges in the region $0.075 \leq x \leq 0.1625$, followed by a second single-phase region when $x \geq 0.175$ which is indexed to an orthorhombic cell of dimensions $\sqrt{2}a_p \times \sqrt{2}a_p \times 2a_p$ (where a_p is the pseudocubic lattice parameter). These materials are second harmonic generation (SHG) active, indicating a non-centrosymmetric structure. A selected area electron diffraction (SAED) experiment performed on the single crystal grain (Figure S3, Supporting Information) on orthorhombic composition $x = 0.20$ along the [010] zone axis (Figure 1e) is consistent with the space groups *Pnam* and $Pna2_1$ and allows us to exclude the other polar subgroups of *Pnam* ($Pn2_1m$ and $P2_1am$). SAED experiments cannot distinguish between nonpolar *Pnam* and polar $Pna2_1$ because they have the same reflection conditions: convergent beam electron diffraction (CBED), which is a powerful and definitive tool for point symmetry determination, was therefore employed to distinguish between their respective *mmm* and *mm*2 point symmetries. The CBED pattern corresponding to the SAED pattern along the [010] zone axis is shown in Figure 1f. In this zone axis, two mirror planes are expected for *Pnam* whereas only one mirror plane is expected for $Pna2_1$.[11] Only one mirror plane is observed in the CBED pattern which confirms that the space group is $Pna2_1$; this absence of inversion symmetry is also confirmed by the non-identical structures in the (200) and $(\bar{2}00)$ discs (Figure 1f). SAED and CBED experiments on the [130] zone axis are also consistent with the non-centrosymmetric structure (see Figure S5, Supporting Information). Thus the structure of $x = 0.20$ is unambiguously confirmed to be $Pna2_1$, described in terms of tilts and displacements as $a_0^-a_0^-c_+^+$,[4] and is denoted $O_{[001]}$ hereafter, as the determined symmetry requires the polarization to lie along the $[001]_p$ cell edge direction. All the compositions with the orthorhombic structure are SHG active and have PXRD patterns consistent with $Pna2_1$ symmetry (Figure S2, Supporting Information). We therefore conclude that the compositions $0.175 \leq x \leq 0.40$ possess a polar orthorhombic structure ($O_{[001]}$) in space group $Pna2_1$ with the polarization along $[001]_p$. The polarization is thus in the same direction as for $T_{[001]}$ $PbTiO_3$ with respect to the primitive perovskite cell, but the BO_6 octahedra are tilted to produce the expanded orthorhombic cell.

In the compositional range $0.075 \leq x \leq 0.1625$, the PXRD patterns could not be indexed with either $R_{[111]}$ or $O_{[001]}$ structures (Figure S6a,b, Supporting Information). Two-phase Lebail fits based on ($R_{[111]} + O_{[001]}$) resulted in good fits to the data with all peaks indexed (Figure 1b and Figure S2 and S6c, Supporting Information), consistent with a mixed phase structure ($R_{[111]} + O_{[001]}$) containing both polarization directions (Figure 1b). All the ($R_{[111]} + O_{[001]}$) compositions are SHG active and lie between two polar phases, confirming that compounds in this region are polar at ambient temperature. Detailed structural characterization of this complex region will be the subject of future study and is expected to be challenging: e.g., the structure of PZT at and near the MPB remains the subject of controversy after many years of detailed study where both multiple and single phase models have been proposed.[12–15]

The reduced lattice parameters ($\sqrt[3]{(V_R/2)}$ for $R_{[111]}$ and $a_O/\sqrt{2}$, $b_O/\sqrt{2}$, $c_O/2$ for $O_{[001]}$, where V_R is the volume of the rhombohedral unit cell and a_O, b_O, c_O are the lattice parameters of orthorhombic unit cell) correspond to pseudocubic cell dimensions and are plotted against CTO content x in Figure 1d. From the diffraction patterns and lattice parameter variation, the phase boundaries are clearly visible around $0.05 < x < 0.075$ and $0.1625 < x < 0.175$. The mixed phase region spans $\Delta x \approx 0.088$ and is of comparable width to those reported for the MPB region of PZT ($\Delta x \approx 0.01$–0.15)[16,17] and other Pb-free MPB systems (0.08 for NBT–KBT,[18] 0.01 for NBT–BTO[19]).

To examine the piezoelectric behavior, discs were poled and longitudinal piezoelectric coefficients (d_{33}) were measured across the full range of compositions ($0 \leq x \leq 0.40$: **Figure 2**a). Compositions with the $R_{[111]}$ structure show an increase in d_{33} with increasing x. Compositions with the $O_{[001]}$ structure showed small finite d_{33} values consistent with their polar structures. The d_{33} value increases with decreasing x in the "$O_{[001]}$" region, reaching a maximum of 2.8 pC N^{-1} at $x = 0.1875$. Most interestingly, d_{33} increases sharply near the phase boundaries and a maximum d_{33} of 53 pC N^{-1} is found for $x = 0.1625$. This is about two orders higher than found for the parent R phase BTFM (0.65 pC N^{-1})[20] and a quarter of that of PZT (223 pC N^{-1}).[1] Despite being polar, the polarization–electric field ($P(E)$) measurements on single phase $R_{[111]}$ ($x = 0.05$) and $O_{[001]}$ ($x = 0.20$) materials did not result in saturated loops (Figure 2b,d). This indicates that the coercive field is much higher than the measurement fields (150–200 kV cm^{-1}) accessed here. In sharp contrast, all the mixed phase compositions showed saturated $P(E)$ loops (Figure 2c shows data for $x = 0.10$). This agrees well with the maximized d_{33} in the mixed phase region. Transverse piezoelectric coefficient (d_{31}), planar coupling coefficient (k_p), elastic compliance (s_{11}^E), and mechanical quality factor (Q_{31}) were calculated from radial extensional resonance mode on poled discs as shown in Figure 2e. For $x = 0.15$ ($R_{[111]} + O_{[001]}$), d_{31}, k_p, s_{11}^E, and Q_{31} are 7 pC N^{-1}, 0.12, 8.25×10^{-12} m^2 N^{-1}, and 360, respectively (see Table S2, Supporting Information for other compositions and comparison with PZT and other lead-free MPB systems). In particular, the mechanical quality factor (Q_{31}) which is important for high power applications,[21] reaches a maximum

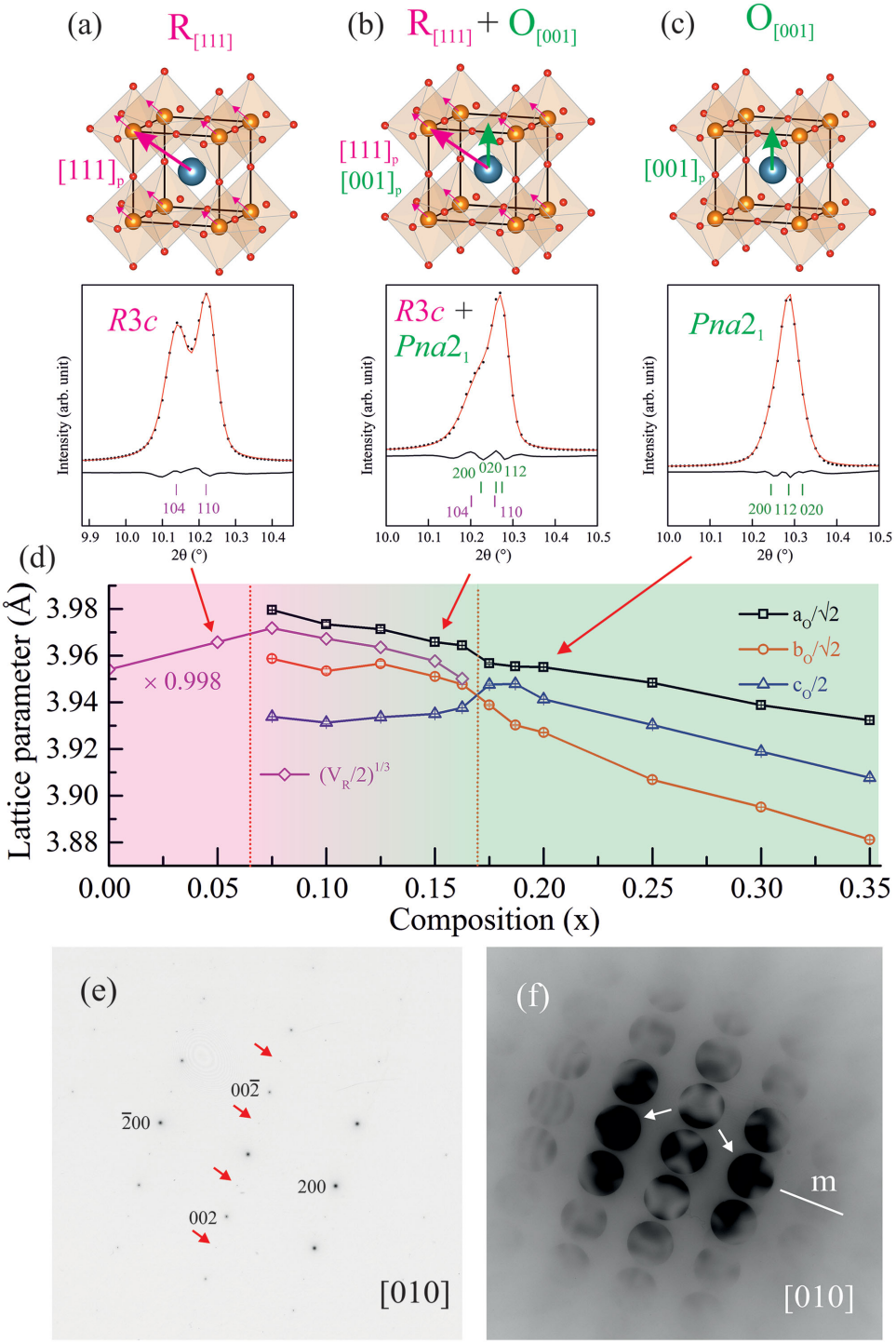

Figure 1. a–c) Lebail fits to $x = 0.05$ ($R_{[111]}$), $x = 0.15$ ($R_{[111]}$+ $O_{[001]}$), and $x = 0.20$ ($O_{[001]}$), respectively (the most intense $[110]_p$ cubic perovskite peaks, where p subscript indicates that the Miller indices refer to the cubic perovskite sub cell, are shown for clarity) with corresponding schematic unit cell diagrams showing the polarization directions present in the $R_{[111]}$, ($R_{[111]}$ + $O_{[001]}$), and $O_{[001]}$ structures in the cubic perovskite sub cell, where the arrows indicate the polarization directions of A-site cations (blue atoms) and B-site cations (orange atoms), with the oxide sublattice (red atoms) defining the shaded BO_6 octahedra. d) Room-temperature lattice parameters obtained from Lebail fits to synchrotron PXRD data plotted against composition (x), showing the structural transition from $R_{[111]}$ (area shaded in pink) to $O_{[001]}$ (area shaded in green) with a region of phase coexistence at $0.075 \leq x \leq 0.1625$. The red arrows indicate the compositions plotted in (a)–(c). e) SAED pattern from $x = 0.20$ ($O_{[001]}$) along the [010] zone axis, which is consistent with *Pnam* and *Pna*2_1. The red arrows indicate spots from double diffraction (see tilt experiment results in Figure S4, Supporting Information). f) Corresponding CBED pattern along the [010] zone axis showing the presence of a single mirror plane confirming the *Pna*2_1 space group. The arrows indicate the (200) and ($\bar{2}$00) discs: the different appearances of these discs are consistent with non-centrosymmetry.

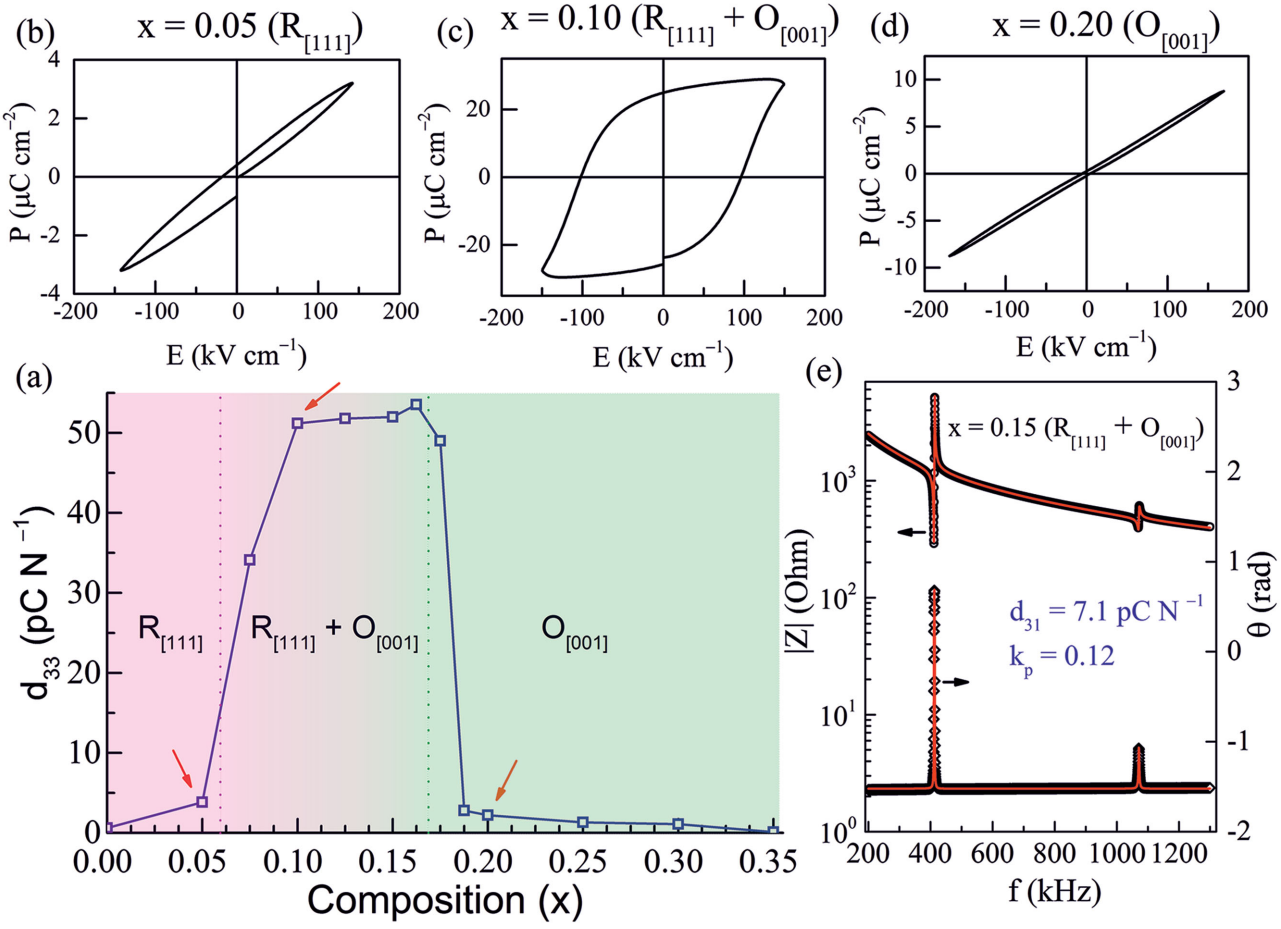

Figure 2. a) Variation of longitudinal piezoelectric coefficient (d_{33}) with CTO content (x) on poled ceramic pellets. Compared to the low d_{33} values ($d_{33} < 4$ pC N^{-1}) of single-phase $O_{[001]}$ and $R_{[111]}$ materials, the mixed phase ($R_{[111]} + O_{[001]}$) compositions show enhanced d_{33} values (52 pC N^{-1} for x = 0.15). b–d) $P(E)$ loops under comparable measurement fields for $R_{[111]}$ (x = 0.05), $R_{[111]} + O_{[001]}$ (x = 0.10) and $O_{[001]}$ (x = 0.20) materials, respectively (indicated by the red arrows). e) Impedance and phase plotted against frequency on a poled thin disc of x = 0.15 showing radial extensional resonance modes. The open symbols and lines represent measured and fitted data, respectively.

of 460 for x = 0.075, comparable to PZT (Q_M = 500)[1] and considerably higher than several established Pb-free MPB systems (see Table S2, Supporting Information).[2,3]

The ($R_{[111]} + O_{[001]}$) composition x = 0.15 was selected for a detailed study of electromechanical properties in the MPB region. Room temperature $P(E)$ loops at a frequency of 1 Hz (preset delay = 1 s) under different measurement fields are shown in **Figure 3**a. Well saturated loops are obtained with the maximum polarization (P_{max}), remanent polarization (P_{rem}) and coercive field (E_C) of 49 μC cm^{-2}, 44 μC cm^{-2}, and 110 kV cm^{-1}, respectively. The remanent polarization observed is higher than that of PZT ceramics (P_{rem} = 35 μC cm^{-2}) and other lead-free ceramics at the MPB.[2,3] To verify the large observed polarization, PUND (positive-up-negative-down) measurements were performed with square pulses (pulse width = 1000 ms and pulse delay = 1000 ms). A switchable polarization of $P \approx$ 49 μC cm^{-2} is obtained (Figure 3c) and this confirms that large polarization is intrinsic. Room temperature strain-field measurement on the same composition at 1 Hz exhibited the classic butterfly loop (Figure 3b). The saturated $P(E)$ loops and the butterfly strain-field data demonstrate the ferroelectric nature of this material. The observed bipolar strain of 0.16% is of the same order as PZT (0.30%).[3] Saturated $P(E)$ and butterfly strain-field loops are observed for all ($R_{[111]} + O_{[001]}$) compositions. The discs have low dielectric loss (tan$\delta \approx$ 0.03 at 1 Hz) that supports measurements up to fields of 200 kV cm^{-1}.

To correlate the Berlincourt d_{33} value with the direct piezoelectric coefficient, unipolar strain-field loops were measured (Figure 3d). The piezoelectric coefficient calculated from the low field slope is 46 pC N^{-1} which is close to the Berlincourt value of 52 pC N^{-1}. The effective piezoelectric coefficient (d^*_{33} = 77 pC N^{-1}) is slightly higher than the observed d_{33}. The unipolar loop exhibited non-linearity with a hysteresis (h) of 27%. The finite hysteresis and mismatch of d_{33} and d^*_{33} may indicate an irreversible contribution from domain wall motion.[2,3]

The composition x = 0.175 (single phase $O_{[001]}$ before poling) showed a d_{33} (49 pC N^{-1}) close to the mixed phase compositions (Figure 2a). X-ray diffraction on a poled disc of x = 0.175 shows the appearance of peaks corresponding to the $R_{[111]}$

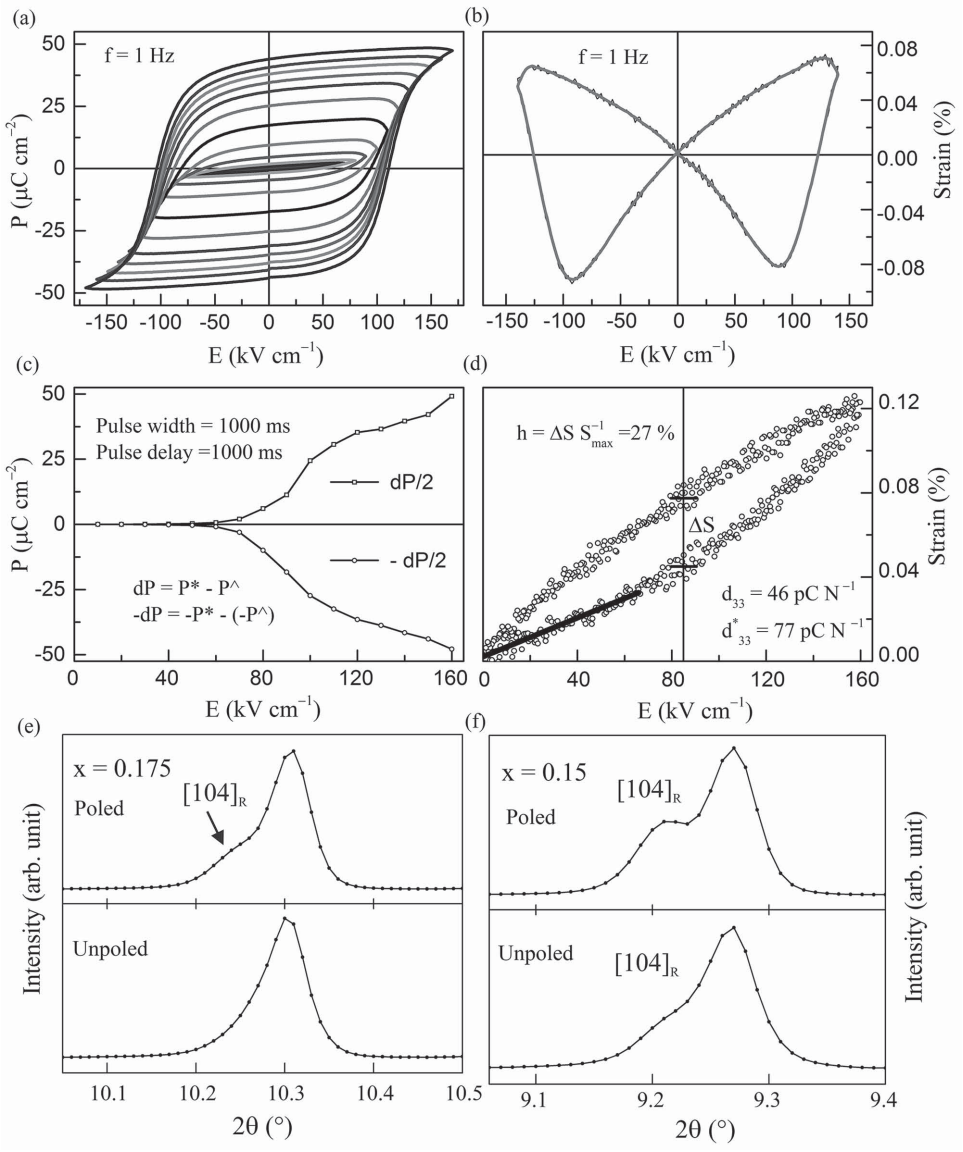

Figure 3. Room temperature electromechanical properties of an ($R_{[111]} + O_{[001]}$) composition $x = 0.15$. a) Saturated $P(E)$ hysteresis loops and b) butterfly strain-field loop at 1 Hz confirming ferroelectricity. c) PUND measurement confirming the polarization value. P^* contains remanent and non-remanent polarizations whereas $P^\wedge$ contains non-remanent polarization contributions. dP ($= P^* - P^\wedge$) represents the remanent polarization. d) Unipolar strain-field loop showing d_{33} (calculated from the low field slope as shown by the black line) and effective d^*_{33} ($=S_{max}/E_{max}$, where S_{max} is the strain observed at the maximum field E_{max}) and finite hysteresis h ($= \Delta S/S_{max}$; where ΔS is the width of the widest part of the loop). e,f) PXRD patterns, plotted over the 2θ range which contains the most intense $[110]_p$ cubic perovskite subcell reflections (similar to Figure 1a–c), from unpoled (bottom panels) and poled (top panels) pellets of $x = 0.175$ ($O_{[001]}$) and $x = 0.15$ ($R_{[111]} + O_{[001]}$), respectively. The increase in the intensity of the rhombohedral [104] peak, which is clearly resolved, indicates that an electric field-induced change in polarization direction occurs in the MPB region. Incident wavelengths are 0.45018 and 0.499953(9) Å for $x = 0.175$ and $x = 0.15$, respectively.

phase, indicating a change in polarization direction under electric field (Figure 3e).[22] This is also evident from the change in the relative intensities of the $R_{[111]}$ and $O_{[001]}$ components of the $x = 0.15$ composition after poling (Figure 3f).

For practical applications, temperature stability of piezoelectric properties and high Curie temperature (T_C) are advantageous. Recently, it has been suggested that the depolarization temperature (T_d) is more relevant since in many systems partial or complete loss of polarization occurs at T_d which can be well below T_C.[2,5] T_d has been estimated from the temperature dependence of d_{33} measured ex situ. For $x = 0.10$ ($R_{[111]} + O_{[001]}$), d_{33} drops sharply to a low value (≈1 pC N^{-1}) at $T_d = 650$ °C and becomes zero at $T_C \approx 840$ °C (Figure S7, Supporting Information). Changes in the diffraction patterns support the depolarization at T_d whereas the Curie temperature is supported by differential scanning calorimetry (DSC) and dielectric permittivity data (Figure S7, Supporting Information). These experiments indicated that

depolarization occurs below T_C in all the ($R_{[111]}$ + $O_{[001]}$) compositions (Table S2, Supporting Information). The composition $x = 0.10$, with a room temperature d_{33} of 50 pC N^{-1} and T_d of 650 °C, which is high for a Pb-free MPB system (Table S2, Supporting Information),[2,5] is therefore of interest for high temperature piezoelectric applications. The origin of the depolarization and the detailed phase diagram versus temperature is the subject of further study.

We have stabilized a perovskite with polarization directed along the $[001]_p$ primitive cell edge that has a high bismuth content (up to 92.5% bismuth on the A-site cf., KBT[23]) and is accessible at ambient pressure (cf., $BiInO_3$[24]). The mixed phase region with the polar $R_{[111]}$ phase generates an MPB reminiscent of that in PZT, based on Bi-rich $R_{[111]}$ and $O_{[001]}$ structures. A piezoelectric coefficient d_{33} of 52 pC N^{-1}, mechanical quality factor Q_{31} of 460, a switchable polarization of 49 μC cm^{-2}, and a depolarization temperature T_d of up to 650 °C were observed for bulk ceramics in the MPB-like composition range. The new Pb-free MPB system offers the opportunity for further electromechanical property improvement by chemical substitution and strain optimization.

Experimental Section

High quality powder samples were synthesized by a conventional solid-state reaction of binary oxide and carbonate precursors heated at temperatures of 900–950 °C for 12 h (described in detail in Table S1, Supporting Information). Phase purity was confirmed using a PANalytical X'pert Pro diffractometer (Co $K\alpha_1$, λ = 1.78896 Å). High resolution PXRD data were collected on beamline BL44B2[25] at SPring-8 with an incident wavelength λ = 0.499953(9) Å in Debye–Scherrer geometry with samples contained in spinning glass capillaries. This instrument was also used to collect data from poled and unpoled pellets of approximate thickness 180 μm (x = 0.15) and 80 μm (x = 0.175), which were contained in a rocking sample holder. Lattice parameters were extracted from Lebail fits in the 2θ range $3 \leq 2\theta \leq 74°$. For synchrotron diffraction experiments at high temperature (30–700 °C), powder samples were packed in a 0.1 mm quartz capillary and data were collected from the I11 powder diffractometer at the Diamond Light Source, with an incident wavelength of 0.825725 Å.[26] Electron diffraction experiments (SAED and CBED) were conducted using a JEOL 2000FX electron microscope operating at 200 kV. Analysis was performed on a single crystal grain (Figure S3, Supporting Information) in a thin lamella specimen prepared by the lift out method[27] using a dual beam FEI focused ion beam instrument; final milling steps were performed using an 8 kV Ga ion beam. Powder second-harmonic generation (SHG) measurements were performed on a modified Kurtz-non-linear optical system using a pulsed Nd:YAG laser with a wavelength of 1064 nm.[28]

Physical property measurements were performed on pellets with densities greater than 95% of the crystallographic values, which were produced from high quality powders by ball-milling, isostatic pressing, and a final sintering step (these processing conditions are described in detail in the Supporting Information). Pellet densities were measured using an Archimedes balance and their phase purity was confirmed by laboratory PXRD. Thin discs (100–200 μm) electroded with silver paint or sputtered gold were poled at 150–200 °C for 10 min under 100 kV cm^{-1} field. Piezoelectric coefficients (d_{33}) were measured using a d_{33} piezometer and other electromechanical properties (d_{31}, k_p, s^E_{11}, Q_{31}) were measured using resonance–antiresonance method. Impedance and phase angle were measured using an Agilent E4980 inductance–capacitance–resistance (LCR) meter and HP4294A impedance analyzer. Polarization and strain-field loops were collected at 1 Hz using a Radiant ferroelectric tester system coupled with Fotonic sensor MTI-2100. Short-circuited poled pellets were depoled at a selected temperature and d_{33} was measured ex situ using the piezometer. DSC experiments were performed using an SDT Q600 instrument with a heating and cooling rate of 10 °C min^{-1}. Further details on sample preparation, ceramic processing, SHG experiments, and characterizations are provided in the Supporting Information.

Supporting Information

Supporting Information is available from the Wiley Online Library or from the author.

Acknowledgements

The authors thank the European Research Council (ERC Grant agreement 227987 RLUCIM), the European Union (SOPRANO project Grant No. PITN-GA-2008-214040) and the Engineering and Physical Sciences Research Council (EP/H000925) for support. A.M.-S., E.N., and M.T. thank RIKEN International Program Associate (IPA) for support and Dr. Kato for experimental help at SPring-8 BL44B2. The synchrotron radiation experiments were performed at BL44B2 in SPring-8 with the approval of RIKEN. The authors thank Dr. C. Murray and Dr. C. Tang for assistance on beamline I11 (Diamond Light Source, UK). L.F.H. thanks the European Union (NANOMOTION project Grant No. 290158). T.T.T. and P.S.H. thank the Welch Foundation (Grant E-1457) for support.

Received: November 28, 2014
Revised: February 2, 2015
Published online: March 26, 2015

[1] B. Jaffe, W. R. Cook, H. Jaffe, *Piezoelectric Ceramics*, Academic Press, London **1971**.
[2] T. Shrout, S. Zhang, *J. Electroceram.* **2007**, *19*, 113.
[3] J. Rödel, W. Jo, K. T. P. Seifert, E.-M. Anton, T. Granzow, D. Damjanovic, *J. Am. Ceram. Soc.* **2009**, *92*, 1153.
[4] H. T. Stokes, E. H. Kisi, D. M. Hatch, C. J. Howard, *Acta Crystallogr. B* **2002**, *58*, 934.
[5] O. L. Serhiy, E. E. Richard, *Sci. Technol. Adv. Mater.* **2010**, *11*, 044302.
[6] S. Zhang, F. Yu, *J. Am. Ceram. Soc.* **2011**, *94*, 3153.
[7] H. Hughes, M. M. B. Allix, C. A. Bridges, J. B. Claridge, X. Kuang, H. Niu, S. Taylor, W. Song, M. J. Rosseinsky, *J. Am. Chem. Soc.* **2005**, *127*, 13790.
[8] C. A. Bridges, M. Allix, M. R. Suchomel, X. Kuang, I. Sterianou, D. C. Sinclair, M. J. Rosseinsky, *Angew. Chem. Int. Ed.* **2007**, *46*, 8785.
[9] S. Y. Chong, R. J. Szczecinski, C. A. Bridges, M. G. Tucker, J. B. Claridge, M. J. Rosseinsky, *J. Am. Chem. Soc.* **2012**, *134*, 5836.
[10] M. R. Dolgos, U. Adem, A. Manjón-Sanz, X. Wan, T. P. Comyn, T. Stevenson, J. Bennett, A. J. Bell, T. T. Tran, P. S. Halasyamani, J. B. Claridge, M. J. Rosseinsky, *Angew. Chem. Int. Ed.* **2012**, *51*, 10770.
[11] D. B. Williams, C. B. Carter, *Transmission Electron Microscopy: Diffraction II*, Plenum Press, New York **1996**.
[12] R. Guo, L. E. Cross, S. E. Park, B. Noheda, D. E. Cox, G. Shirane, *Phys. Rev. Lett.* **2000**, *84*, 5423.
[13] J. Frantti, *J. Phys. Chem. B* **2008**, *112*, 6521.
[14] Y. Zhang, D. Xue, H. Wu, X. Ding, T. Lookman, X. Ren, *Acta Mater.* **2014**, *71*, 176.

[15] N. Zhang, H. Yokota, A. M. Glazer, Z. Ren, D. A. Keen, D. S. Keeble, P. A. Thomas, Z. G. Ye, *Nat. Commun.* **2014**, *5*, 5231.
[16] P. Ari-Gur, L. Benguigui, *Solid State Commun.* **1974**, *15*, 1077.
[17] M. R. Soares, A. M. R. Senos, P. Q. Mantas, *J. Eur. Ceram. Soc.* **1999**, *19*, 1865.
[18] M. Otoničar, S. D. Škapin, M. Spreitzer, D. Suvorov, *J. Eur. Ceram. Soc.* **2010**, *30*, 971.
[19] J. E. Daniels, W. Jo, J. Rödel, J. L. Jones, *Appl. Phys. Lett.* **2009**, *95*, 032904.
[20] M. Dolgos, U. Adem, X. Wan, Z. Xu, A. J. Bell, T. P. Comyn, T. Stevenson, J. Bennett, J. B. Claridge, M. J. Rosseinsky, *Chem. Sci.* **2012**, *3*, 1426.
[21] S. Zhang, R. Xia, L. Lebrun, D. Anderson, T. R. Shrout, *Mater. Lett.* **2005**, *59*, 3471.
[22] J. F. Daniel, S. Yo-Han, J. S. Andrew, Z. Yichi, G. Julia, E. D. John, K. Jurij, B. Andreja, M. Barbara, G. W. Kyle, *Sci. Technol. Adv. Mater.* **2014**, *15*, 015010.
[23] G. O. Jones, J. Kreisel, P. A. Thomas, *Powder Diffr.* **2002**, *17*, 301.
[24] A. A. Belik, S. Y. Stefanovich, B. I. Lazoryak, E. Takayama-Muromachi, *Chem. Mater.* **2006**, *18*, 1964.
[25] K. Kato, R. Hirose, M. Takemoto, S. Ha, J. Kim, M. Higuchi, R. Matsuda, S. Kitagawa, M. Takata, *AIP Conf. Proc.* **2010**, *1234*, 875.
[26] S. P. Thompson, J. E. Parker, J. Potter, T. P. Hill, A. Birt, T. M. Cobb, F. Yuan, C. C. Tang, *Rev. Sci. Instrum.* **2009**, *80*, 075107.
[27] L. A. Giannuzzi, F. A. Stevie, *Micron* **1999**, *30*, 197.
[28] K. M. Ok, E. O. Chi, P. S. Halasyamani, *Chem. Soc. Rev.* **2006**, *35*, 710.